Experimental observation of thermoacoustic turbulence and universal properties at the quasiperiodic transition to chaos

T. Yazaki*
Department of Physics, Aichi University of Education, Igaya-cho, Kariya-shi, Aichi-ken 448, Japan
(Received 31 August 1992; revised manuscript received 15 March 1993)

In this paper, we report experimental results of strongly nonlinear phenomena observed in the thermoacoustic system which we have termed "Taconis oscillation" [W. H. Keesom, *Helium* (Elsevier, New York, 1942), p. 174; C. F. Squire, *Low Temperature Physics* (McGraw-Hill, New York, 1953), p. 23; K. W. Taconis, J. J. M. Beenaker, A. O. C. Nier, and L. T. Aldrich, Physica **15**, 733 (1949) (see footnote on p. 738)]. The system exhibits quasiperiodic and chaotic dynamics in spontaneous states and states forced by external oscillation. In spontaneous states, we observed that three clearly defined stable modes with incommensurate frequencies can be excited simultaneously, and that competition between them leads to chaotic motion near the overlapping regions of the stability curves. Experimental time series of chaotic oscillations are analyzed by theories of nonlinear dynamical systems, and the dimension and entropy of chaotic attractors are determined. In forced thermoacoustic states, a spontaneous oscillation is periodically perturbed by a mechanical force with amplitude and frequency externally controlled. Nonlinear coupling between thermally and mechanically driven oscillators leads to quasiperiodicities, frequency-locking, and the onset of chaos within a certain bandwidth. The global and local universal properties for the quasiperiodic transition to chaos are experimentally studied and compared with circle map universality. We present experimental results for universal scaling properties at the onset of chaos in order to examine the applicability of the map to certain aspects of thermoacoustic systems such as (1) the self-similar hierarchical structure and scaling power spectrum at a particular winding number (the golden mean), (2) the fractal dimension of the set of locked states on the critical line, and (3) the multifractal spectrum. In particular, the scaling power law of the spectrum is found to change from f^4 to f^2 as the system approaches the onset of chaos. We provide numerical support for the hypothesis that the change of the scaling power law is attributed to the drastic change of the Poincaré cross section from a mild to a sharp wrinkle. The experiment demonstrates that the thermoacoustic system belongs to the same universality class as the simple map, at least up to the onset of chaos, in spite of the complexity of the system.

PACS number(s): 47.27.Cn, 05.45.+b, 05.70.Ln, 43.90.+v

I. INTRODUCTION

Some thermoacoustic phenomena such as the Sondhauss tube [1] and the Rijke tube [2] have received considerable attention for over two centuries. The progress of research on these phenomena, however, was slow because of the great complexities of the system and the lack of systematic experiments. In recent years, there has been a growing interest in the concept of thermoacoustics in connection with the fields of nonlinear dynamics and applications [3].

The thermoacoustic system which attracted our interest is the self-sustained oscillation of a thermally induced cryogenic gas column. When a gas column confined in a long cylindrical tube is subjected to strong temperature gradients, its spontaneously oscillates with extremely large amplitudes ($\sim 10^4$ Pa or more). We have termed this the "Taconis oscillation" [4], which is a classic thermoacoustic phenomenon where some heat is converted to work under certain conditions. Recently, thermoacoustic oscillations have been studied in terms of hydrodynamics and thermodynamics. Rott [5] gave the theoretical phase diagram for hydrodynamics between oscillation and no oscillation, and this was experimentally confirmed by Yazaki, Tominaga, and Narahara [6] to be valid within a small-amplitude region. Swift [7] and Tominaga, Narahara, and Yazaki [8], who reviewed thermodynamics, presented a qualitative understanding of thermoacoustics, some important parameters for the production of sounds by heat, and the essential principle of an acoustically driven refrigerator as applications of thermoacoustics.

In a certain bandwidth of the stability curve, the Taconis-oscillation system provides us with abundant nonlinear phenomena such as quasiperiodicity, frequency locking, and chaos. In this paper, we present experimental studies of highly nonlinear phenomena associated with thermoacoustic turbulence in spontaneous states and universal scaling properties for the quasiperiodic transition to chaos in externally forced states. Some of the results have already been reported in previously published Letters [9].

In this study, the mechanism of chaotic behavior is shown to arise from competition between different modes of oscillation in a gas column. Stability curves for three different oscillatory modes intersect with each other on the phase diagram. Near the overlapping region and the intersection of the stability curves, three or two modes with incommensurate frequencies can be excited simultaneously, and competition between them leads to chaotic motion (thermoacoustic turbulence) through complex quasiperiodic routes. Two routes to chaos through three-

and two-frequency quasiperiodicities are experimentally identified. While the ability of three-frequency quasiperiodicity to exist stably has been theoretically questioned, our experimental system shows that a stable oscillating flow consisting of three incommensurate frequencies exists before chaotic motion is observed. Numerical experiments done by Grebogi, Ott, and Yorke [10] have demonstrated that a stable three-frequency state exists, especially in conjunction with small nonlinear perturbations. In a few experimental systems [11], the observation of such a state has also been reported. Observed nonperiodic time series which are developed from the two routes are reconstructed and analyzed using nonlinear dynamical theories. The dimension and entropy of chaotic attractors are calculated to give experimental evidence of deterministic chaos [12].

When an oscillating system with one characteristic mode is periodically perturbed by a second oscillator and the two modes nonlinearly interact with each other, the system exhibits abundant nonlinear phenomena. For a small nonlinearity, oscillators are in a quasiperiodic state or a locked state if the ratio of their frequencies (or winding number) is irrational or rational, respectively. As the degree of nonlinearity increases, locked regions become stable over a wide bandwidth of the applied frequency and form "Arnol'd tongues" in the phase diagram. A stronger force leads to the onset of chaos and a hysteretic effect which occurs in the overlapping regions of the tongues. Some of these features related to nonlinear coupling between two modes are common to many physical systems [13], mechanical oscillators [14], driven electrical oscillators [15], forced convective flow systems [16,17], and solid-state physics [18]. The possibility exists that the quantitative behaviors of a natural oscillation system subjected to a periodic force may be described by a one-dimensional circle map. The following is a typical model called the sine circle map:

$$\theta_{n+1}=\theta_n+\Omega_0-\frac{K}{2\pi}\sin(2\pi\theta_n)\ , \tag{1}$$

where two control parameters K and Ω_0 correspond to the degree of nonlinearity and the unperturbed winding number, respectively. For the transition from quasiperiodicity to chaos ($K=1$) two types of scaling universality have been theoretically predicted by means of numerical and renormalization group techniques [19,20]: one type is the local scaling universality seen in the critical power spectrum at a particular winding number, the golden mean $\sigma=(\sqrt{5}-1)/2$ which has the slowest possible convergence, and the other is the global type for the whole range of winding numbers on the critical line, the fractal dimension D of a devil's staircase. The global scaling universality of the attractors is characterized by the multifractal spectrum [21], which is also predicted by the circle map for trajectories on the critical golden torus. The relevance of the map universality has already been tested and supported in a few experimental systems such as Rayleigh-Bénard convection [13,16,17] and solid-state physics [18].

We would like to experimentally verify whether the map universality is applicable to complex nonlinear thermoacoustic systems. An external periodic force is used as a second oscillator to perturb a natural internal oscillator. Parameters K and Ω_0, which are directly related to the amplitude and frequency of the external force, can be controlled with high accuracy. We present experimental results for universal scaling properties at the onset of chaos to examine the relevance of the map to thermoacoustic systems: (1) the self-similar hierarchical structure and scaling power spectrum at the golden mean, (2) the fractal dimension of the set of locked states on the critical line, and (3) the multifractal spectrum. The experiment demonstrates that a complex thermoacoustic system belongs to the same universality class as the simple map. No matter how complex physical systems are or even if basic equations characterizing nonlinear systems are not known, the behavior of the system at the onset of chaos can be described effectively by the scaling universality predicted by the circle map.

We also report experimental observations for strong forcing, where the dynamical behavior is complex. If spontaneous oscillation does not have a high enough amplitude, the excitation dominates the behavior of the flow before the transition to chaos takes place. A similar phenomenon has also been observed in a forced Rayleigh-Rénard convection [17] and a driven nonlinear spin-wave system [22].

The purpose of this paper is to give detailed experimental results of nonlinear thermoacoustic phenomena partially containing our preliminary results previously published [9]. This paper is organized as follows. In Sec. II we describe briefly our experimental setup and experimental phase diagram. In Sec. III we give experimental results on thermoacoustic turbulence in spontaneous states and on universal scaling properties at the onset of chaos in externally forced states. In Sec. IV we discuss experimental results regarding the change of the scaling power law seen in the envelope of spectral peaks. In the last section, we summarize our conclusions.

II. EXPERIMENT

A. Experimental setup

The experimental arrangement of Taconis oscillation is schematically shown in Fig. 1. Helium gas was confined in a long cylindrical tube with a symmetrical steplike temperature distribution along its axis. A gas column in the tube consists of three sections, homogeneous temper-

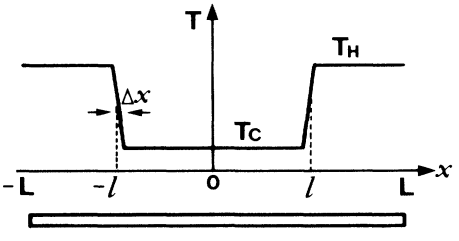

FIG. 1. Mean temperature distribution along the tube closed at both ends.

atures (warm, T_H, and cold, T_C), and abrupt temperature-jump regions at $x=\pm l$. The warm part T_H was maintained at room temperature ($\simeq 296$ K) and T_C was U shaped at $X=0$ and could be varied continuously from $T_C=4.2$ K to about 45 K using the continuous-gas-flow method [6]. The tubes used were stainless steel with inner radii of $r=1.2$, 2.2, and 3.7 mm, wall thicknesses of 0.3 mm, and whole tube lengths of $2L=2.1-2.9$ m. The length Δx with a temperature jump was less than 4% of the tube length. Mean density of the helium gas was continuously varied through a capillary tube attached to the gas column. Acoustic and mean pressures were converted to electrical voltages by two small pressure transducers (Toyoda Koki, Model No. DD102-1F) attached at the two closed ends with excellent linearity over a wide range. The signal voltage $V(t)$ monitored by a spectrum analyzer (Ono Sokki, Model No. CF6400) was digitized by 12-bit analog-to-digital converters. The time series of 16 384 sample points were analyzed by a computer to obtain information on detailed power spectra and attractors in the phase space.

B. Control parameter and phase diagram

Researchers in the field of cryogenics often suggest that the amplitude of Taconis oscillation strongly depends on the inner radius r of the tube. That is, the ability to induce excitation is greatly lessened if the inner radius of the gas column tube is too large or too small. This empirical observation suggests that the dimensionless parameter r/δ is important to control thermoacoustic oscillation. The intrinsic parameter δ represents the thermal boundary layer thickness $\sim\sqrt{\alpha/\omega}$ (ω is the angular frequency of the oscillation and α is the thermal diffusivity of the gas) formed at a tube wall. At least one of parameters controlling the amplitude of Taconis oscillation is given by

$$\frac{r}{\delta}=r\left[\frac{\omega}{\alpha}\right]^{1/2}(=Y)\ . \tag{2}$$

Defining the relaxation time $\tau=r^2/\alpha$ we can rewrite Eq. (2) as

$$Y^2=\omega\tau\ , \tag{3}$$

where τ shows the time delay between the tube wall and oscillating fluid temperatures. If $\omega\tau\ll 1$ (or $r\ll\delta$), then the motion of a fluid in a tube becomes isothermal. If $\omega\tau\gg 1$ (or $r\gg\delta$), then the motion becomes adiabatic. In such reversible processes, Taconis oscillation is not excited. When $\omega\tau\simeq 1$ the oscillation can be effectively induced [7,8]. Our experimental apparatus was designed to vary the control parameter, Eqs. (2) or (3), continuously through the mean density of a gas over a wide range.

As Eq. (2) is not well defined in temperature-jump regions, we select the following dimensionless numbers well defined in T_H and T_C to map out the phase diagram, the boundaries of stable and unstable regions:

$$Y_C=r\left[\frac{\omega}{\alpha_C}\right]^{1/2},\quad Y_H=r\left[\frac{\omega}{\alpha_H}\right]^{1/2}, \tag{4}$$

where the subscripts H and C represent warm and cold, respectively. Equation (4), however, is not the independent variable in the experiment because the frequency is not initially known for a given tube. Therefore we reconstructed Eq. (4) and adopted the following new numbers independent of the frequency as control parameters:

$$R=\frac{Y_C}{\sqrt{\lambda}},\quad \frac{T_H}{T_C}=\left[\frac{Y_C}{Y_H}\right]^{2/1+\beta}, \tag{5}$$

where λ is defined by $\omega l/a_C$ (a_C is the adiabatic sound velocity at the cold part) and β is 0.647 for helium gas.

The experimental phase diagram drawn up in the space of Eq. (5) is shown in Fig. 2. Taconis oscillation is spontaneously induced when the temperature ratio exceeds a threshold value which is dependent on R. The time development of the pressure growth was initially exponential and saturated after a few seconds. Neutral points were explored by gradual variation of R through the mean density of a gas at a constant temperature ratio. The control parameter R could cover three orders of magnitude, with large overlap, by changing the mean density and the tube inner radius. The phase diagram is characterized by a united curve which is independent of tube geometry. This means that Eq. (5) is essential to characterize the stability of Taconis oscillation. As pointed out in the beginning of this section, the spontaneous oscillation can be induced in the limited region of $\omega\tau$ above a minimum temperature ratio. There exist two stability limits corresponding to the left- and right-hand branches. A gas needs a suitable thermal boundary layer thickness to maintain the oscillation. The region $\omega\tau\simeq 1$ is in the temperature-jump region, where the driving acoustic energy source exists. Thus, at the left-hand branch it is possible that faster gas motions (higher frequency modes) with thinner boundary layers are induced instead of the fundamental mode. The second and third modes with two and three pressure nodes at T_C were observed near the left-hand branch only. The stability curve of the second mode intersects with that of the fundamental mode at $T_H/T_C\simeq 15$. The intersection of the

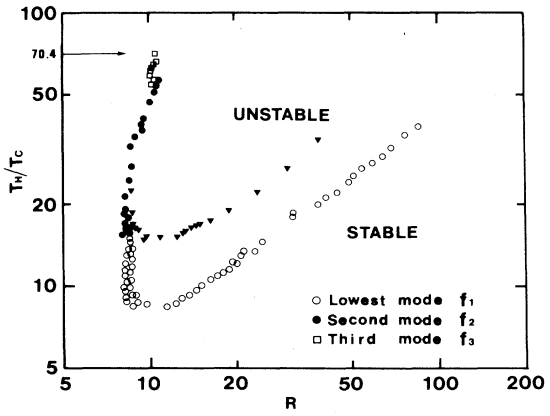

FIG. 2. Experimental phase diagram for $\xi=0.3$ as a function of temperature ratio T_H/T_C vs $R=r(a_C/\alpha_C l)^{1/2}$. Stability limits for an asymmetric tube closed at $X=0$ and L are shown by solid triangles.

curves of the second and third modes was observed at $T_H/T_C \simeq 55$.

Although measurements of the pressures at the two closed ends of the tube provide no direct spatial information, there is some indirect evidence in favor of our determination of the modes. It was confirmed that two pressure wave forms observed at either end were the same in the amplitude and 180° out of phase for the fundamental and third modes, and in phase for the second mode. Appearance of the second mode predicts that a spontaneous oscillation of the fundamental mode can be induced in an asymmetric tube closed at $X=0$. We found the fundamental mode produced in the closed tube, whose stability curve (shown by solid triangles in Fig. 2) coincides closely with that of the second mode (solid circles).

We also observed that the frequency modes that can be thermally excited strongly depend on the location of a temperature jump determined by the ratio between tube lengths of T_H and T_C, $(L-l)/l\,(=\xi)$. Recent theoretical work [8] indicates that the driving energy source is proportional to the product of the mean temperature gradient and the gradient of the square of pressure for the standing acoustic wave (a negative product indicates strongly damped oscillation). The direction of the temperature increase must coincide with that of the pressure increase to maintain oscillation; hence, a gas oscillating tube must be closed at the warm end. The most favorable location for the temperature jump is therefore halfway between a node and a loop. If, for simplicity's sake, the pressure distribution is assumed to be that of a gas column oscillation in a tube with constant temperature, the product reaches a maximum when ξ is 1, 0.33, or 0.2, depending on whether the oscillatory mode is the fundamental, the second, or the third mode. This suggests how many values of ξ we need to select to observe mode competition. The value of $\xi(=0.3)$ used in Fig. 2 enabled us to observe the chaotic mode competition which occurred in the unstable region, where three or two modes are simultaneously induced. For $\xi=0.5$, only two modes, the fundamental and the second, are simultaneously induced when the temperature ratio is less than 70.4, and chaotic mode competition was also observed. The ratio ξ plays an important role in limiting the number of spontaneous modes. For a tube with a large ξ, higher modes are effectively frozen out.

C. Forced thermoacoustic oscillation

In order to study the quasiperiodic transition to chaos at a fixed winding number and to map out Arnol'd tongues, we used the external driving force as one oscillator for experimental convenience. We performed the experiment using the following apparatus and procedure. The value of ξ was 1 in our experimental design (whole tube length 2.8 m, inner radius 1.2 mm), where only the fundamental mode is singled out as a stable excited mode. The spontaneous oscillation was perturbed by an external force whose frequency and amplitude could be continuously and independently varied over a wide range. One closed end of the tube was replaced by a stainless-steel dynamic bellows. A gas column was periodically driven by the bellows attached to a woofer speaker (50 W and 4 Ω impedance), to which an ac voltage, $A_e\sin(2\pi f_e t)$, with the external driving frequency f_e and amplitude A_e, was applied through a power amplifier from a synthesizer (Hewlett-Packard Model No. 3325B). This produces simple harmonic motion in the gas column. The natural oscillator was nonlinearity coupled with the mechanically driven oscillation at the desired winding number and with nonlinearity through the frequency and amplitude of the synthesizer. We could tune the winding number to the golden mean within the accuracy of 10^{-4}. It is essential to keep the winding number constant for comparison with existing models. Nonlinear interaction between two oscillating modes leads to the onset of chaos when their amplitudes are within a certain range.

Real time monitoring of the power spectrum of the signal voltage by a spectrum analyzer on a logarithmic frequency axis enabled us not only to determine the critical point due to an increase in broadband noise level but also to estimate the accuracy with which we can tune the winding number to the golden mean. The main spectral peaks are spaced at regular intervals on a log scale on the frequency axis, and peaks of the first generation can be recognized up to σ^6 near the critical point. Two types of digitized time series of 16 384 points, which were sampled by 2 msec and a period of the external driving force, were recorded with no filter to obtain scaled power spectra and strobed attractors. The determination of a transition point to chaos was also confirmed by the change of a Poincaré cross section from a mild to a sharp wrinkle in addition to an increase in the spectral visible noise floor. The frequency-locking states ($f_1/f_e=p/q$; $q>p$, p and q are integers) were ascertained by counting the number of clumps in the Poincaré cross section on a display unit. The number gives the denominator q. Using this method we could exactly search the 13/21 locking state.

III. EXPERIMENTAL RESULTS

A. Thermoacoustic turbulence in spontaneous states

Chaotic oscillations were investigated at two constant temperature ratios ($T_H/T_C \simeq 70.4$ and 18.4) near the left-hand branch of the phase diagram using a tube with an inner radius of 1.2 mm and a length of 2.9 m. The cold part T_C was always immersed in liquid helium ($T_C=4.2$ K) and T_H was maintained at 296 and 77.3 K (liquid nitrogen). For $T_H/T_C \simeq 18.4$, the periodic motion of the second mode is first excited at $R=7.7$, and a further increase of R leads to the generation of both the fundamental and second modes. Weak nonlinear interaction between the two modes resulted in quasiperiodic motion with smooth modulation, but the chaotic mode competition was not observed when the temperature ratio was so small. Chaotic motion does occur, however, at a higher temperature ratio ($\simeq 70.4$), where the stability curves for three different modes intersect. In the overlapping region, three or two modes can be excited simultaneously, and mode competition leads to chaos. The bifurcation structure leading to chaos was very complex in spontaneous states. We experimentally found two different routes to chaos: three-frequency and two-frequency quasi-

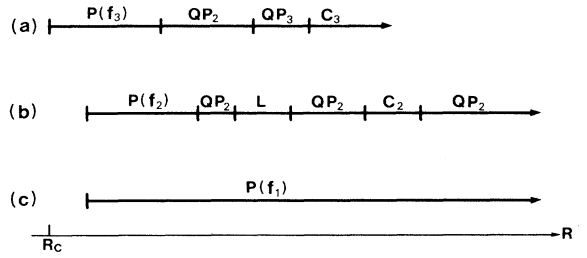

FIG. 3. Schematic representation of the observed routes to chaos as a function of R. (a) Three-frequency quasiperiodic route. The periodic-chaotic sequence follows the periodic state of the third mode $P(f_3)$ spontaneously induced at $R_c=10.4\rightarrow$quasiperiodic state, $QP_2(f_3,f_1)$ or $QP_2(f_3,f_2)$ $\rightarrow$three-frequency quasiperiodicity $QP_3(f_3,f_1,f_2)\rightarrow$chaotic state C_3. (b) Two-frequency quasiperiodic route. The sequence follows the periodic state of the second mode $P(f_2)\rightarrow$quasiperiodic state $QP_2(f_2,f_1)\rightarrow$locking state $L(f_2,f_1)$ with $f_2=2f_1\rightarrow$quasiperiodic state modulated at a low frequency f_m, $QP_2(f_2/2,f_m)\rightarrow$chaotic state $C_2\rightarrow QP_2(f_2,f_1)$. (C) The periodic state of the fundamental $P(f_1)$.

periodicities. The observed sequences, periodic-quasiperiodic-chaotic motions, were classified into two types as schematically shown in Figs. 3(a) and 3(b). The experimental complication comes from the fact that three states, including a periodic state of the fundamental mode [Fig. 3(c)], can be excited for a given R within the restricted limit, and the transitions between them, which are sometimes not reproducible, take place along with hysteretic changes in the control parameter.

1. *Routes to chaos*

As R is increased slowly at $T_H/T_C\simeq 70.4$, a pure periodic oscillation of the third frequency mode $P(f_3)$ is spontaneously generated at $R=10.4$, the left-hand limit of stability in Fig. 2. The value of $\lambda(=4.14)$ indicates that three pressure nodes exist at T_C. The sequence leading to chaos follows the three-frequency route shown in Fig. 3(a). The fundamental mode (sometimes the second mode) increases, and both f_3 and f_1 modes (or f_3 and f_2) are simultaneously induced. The nonlinear interaction between them leads to a quasiperiodic state $QP_2(f_3,f_1)$ [or $QP_2(f_3,f_2)$] where the periodic signal of the third mode is slowly modulated at frequency f_1 (or f_2). The spectrum consists of the sharp peaks of f_3,f_1 (or f_3,f_2) and components of their linear combination. Following the third mode, whether f_1 or f_2 is induced depends on only a slight difference in the location of the temperature jump. Although the frequency ratios of f_1/f_3 and f_2/f_3 are close to $\frac{1}{3}$ and $\frac{2}{3}$, respectively, the frequency-locking state is not observed except in very small widths of locked regions. Before the onset of chaos, we observed a three-frequency quasiperiodic state $QP_3(f_3,f_1,f_2)$ stable enough to be easily detected in the spectrum. The wave form and the corresponding power spectrum including a partially magnified figure are shown in Figs. 4(A), 4(a), and 4(b). All spectral peaks were identified and were described by linear combinations of f_1, f_2, and f_3 within the experimental accuracy of 30 mHz. To confirm that no synchronization between the three modes occurs in the state shown in Fig. 4(A), we calculated the correlation dimension ν (to be discussed later) of the attractor constructed from time series using the embedding method. We obtained $\nu\simeq 3.0$. Furthermore, we ascertained that the Poincaré cross section is not a closed curve. Taconis oscillation exhibits a stable quasiperiodic oscillating flow consisting of three incommensurate frequencies. Chaotic mode competition [Fig. 4(B)], represented by C_3, was observed in a small layer of R after the three-frequency quasiperiodic regime. The corresponding power spectrum in Fig. 4(c) shows the gradual broadening of the spectral peaks. We could not experimentally determine whether chaotic motion follows the three-frequency quasiperiodic state or the two-frequency mode-locked state. If R increases further, the

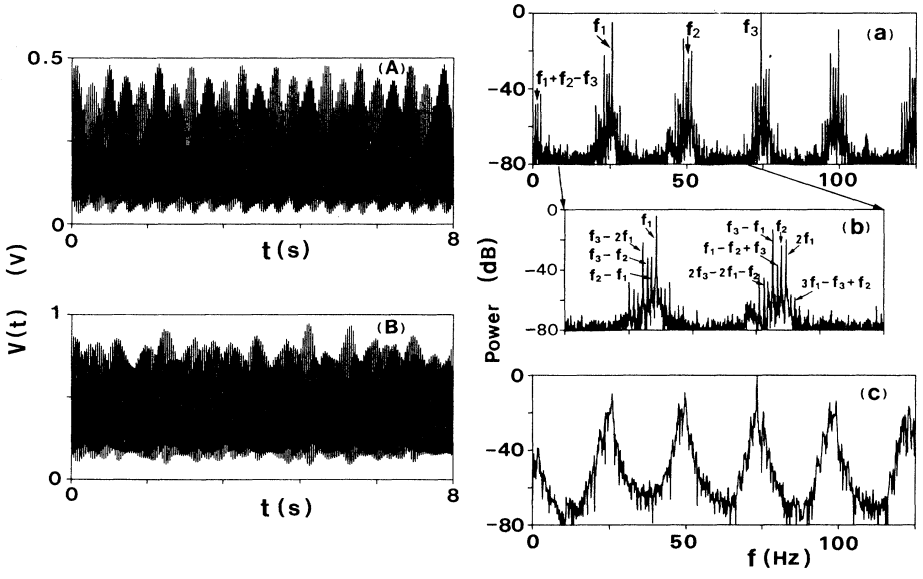

FIG. 4. Pressure records (5.5×10^3 Pa/V) and power spectra of instabilities leading to chaos through three-frequency route: (A) and (a) $R=12.4$, three-frequency quasiperiodic state developed from $QP_2(f_3,f_1)$; (b) partially magnified figure of (a); and (B) and (c) $R=12.9$, chaotic oscillation.

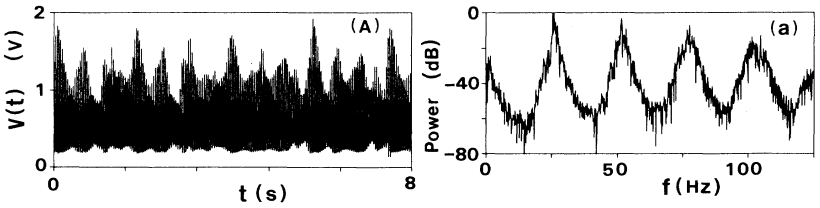

FIG. 5. Pressure record and power spectrum of chaotic state through two-frequency route ($R=13.5$).

third mode is frozen out and the system makes a transition from the chaotic state to a state of the two-frequency route.

The quasiperiodic state $QP_2(f_3,f_1)$ sometimes follows the two-frequency route before the generation of three-frequency quasiperiodicity, normally via the periodic state of the second mode $P(f_2)$. This sequence depends on the history of the system and exhibits hysteresis. When we gradually decreased R after the transition to the second mode, the transition from the second to third mode occurs at a position near the extrapolation line of the stability curve of the second mode without developing quasiperiodicity.

The sequence leading to chaos through the instabilities induced with only two oscillators, the fundamental and second modes, follows the two-frequency route shown in Fig. 3(b). After the periodic state $P(f_2)$ developed into a quasiperiodic state $QP_2(f_2,f_1)$ due to fundamental mode generation with a frequency of about half that of the second mode, we observed frequency locking between f_1 and $f_2(f_2=2f_1)$. As a control parameter increases, modulation of the locked state $L(f_2,f_1)$, which is composed of the spectral peaks of $f_2/2$ and its higher harmonics, begins at a low frequency f_m. The system eventually reaches a smoothly modulated quasiperiodic state $QP_2(f_2/2,f_m)$. The sinusoidal envelope gradually deteriorates, and finally the system exhibits well-developed chaotic motion C_2, whose time record and power spectrum are shown in Figs. 5(A) and 5(a), respectively. The resultant chaotic region is sufficiently wide compared with that of the chaotic three-mode competition. The chaotic motion changes into the quasiperiodic state $QP_2(f_1,f_2)$ with amplitude modulation exhibiting a "cockscomb" pattern, which is characterized by a sudden jump [9]. A further increase of control parameter R leads to smooth modulation and a decrease of the number of spectral peaks, and finally the second mode is frozen out so that only the fundamental mode is excited [Fig. 3(c)]. In large control parameter regions, the gas column oscillates with amplitudes greater than 40% ($\sim 5\times 10^4$ Pa, peak-to-peak value) of the mean pressure.

In such large-amplitude regions, we observed thermally driven shock waves characterized by discontinuity in the slope and a concomitant sudden rise in the pressure. As a result we could not maintain the steplike temperature distribution because of the abnormal heat transport enhanced by the oscillation [23]. Observation of shock waves has also been reported in gas column oscillation mechanically driven by a piston near a resonance frequency [24].

We found a two-frequency state $QP_2(f_2,f_1)$ using a tube with $\xi=0.5$, in which the third mode was frozen out and only two modes, f_1 and f_2, were excited below $T_H/T_C\simeq 70.4$. The observed sequence leading to chaos was essentially the same as the two-frequency route [Fig. 3(b)] observed in the tube with $\xi=0.3$.

2. *Time series analysis of chaotic oscillations*

To document that the nonperiodic oscillations presented in Figs. 4(b) and 5(A) are deterministic chaos, we analyzed the experimental time series using recent methods from theories of nonlinear dynamical systems. Deterministic chaos is characterized by the fundamental quantities of indicators, at least one positive Lyapunov exponent, a finite and positive value of the Kolmogorov entropy, and a fractal dimension of the attractor. Several techniques have been developed for estimating such quantities directly from experimental time series. The experimental determination of the quantities may be useful not only to document deterministic chaos but also to propose an appropriate model equation describing thermoacoustic turbulence.

Assuming that the observed signal is caused by some deterministic nonlinear system with a finite dimension, we can regard the signal as a one-dimensional projection of the trajectory in a multidimensional phase space. A phase projection of dimension m is directly constructed from a single time series $V(t_i)$ using the embedding method [25]. The phase-space coordinates which are topologically equivalent to the portrait of the original system are constructed from the vector

$$(V(t_i),V(t_i+\tau_d),\ldots,V(t_i+(m-1)\tau_d)) ,$$

where τ_d is an arbitrary delay time. Two-dimensional projections of three-dimensional phase portraits which were constructed by plotting the voltages $V(t_i)$, $V(t_i+\tau_d)$, and $V(t_i+2\tau_d)$ are shown in Figs. 6(a) and 6(b) for the experimental data presented in Figs. 5(A) and

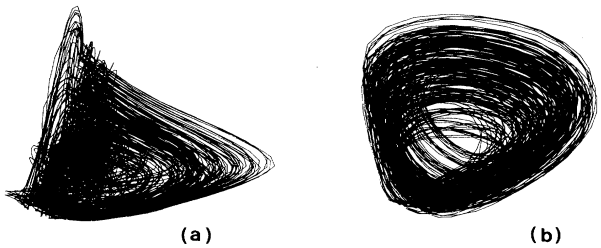

FIG. 6. Two-dimensional projections of three-dimensional phase portraits constructed by plotting of the voltages $V(t_i)$, $V(t_i+\tau_d)$, and $V(t_i+2\tau_d)$: (a) and (b) correspond to Figs. 5(A) and 4(B), respectively.

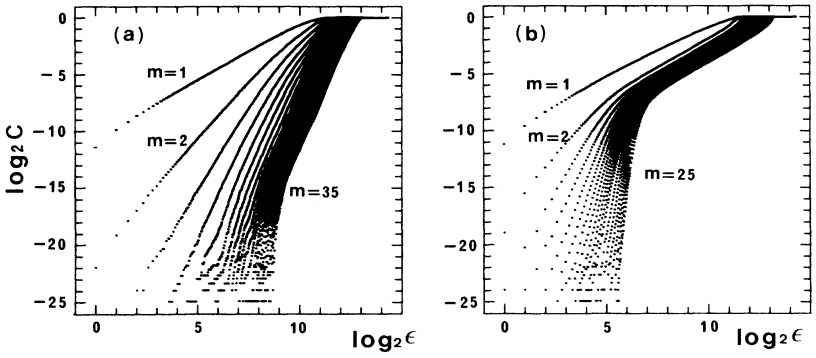

FIG. 7. Log-log plot of correlation integrals $C_m(\epsilon)$ vs radius ϵ of m-dimensional ball: (a) and (b) correspond to chaotic attractor of Fig. 6(b) and a limit cycle of the third mode, respectively. The saturated slope for large m shows the correlation dimension ν of the attractor.

4(B), respectively. The delay time τ_d was set to about $\frac{1}{4}$ of the intrinsic oscillation period. The Poincaré cross sections given by the intersection of trajectories in three-dimensional portraits with a plane are broken down, and yield no useful information.

To obtain phase-space information of such chaotic attractors we adopted the generally accepted method introduced by Grassberger and Procaccia [26] to determine the correlation dimension ν and the entropy K_2. These values are defined in terms of quantities called correlation integrals $C_m(\epsilon)$, which show the number of pairs of data points whose separation is less than ϵ in the phase space of the m-embedding dimension. Because the correlation integrals scale as $\sim\epsilon^{\nu}$ over some range of ϵ, the correlation dimension ν can be determined by

$$\nu=\lim_{\epsilon\to 0}\frac{\log_2 C_m(\epsilon)}{\log_2\epsilon}$$

which is an approximation of the fractal dimension. Using about 8500 sampling points, we calculated $C_m(\epsilon)$ for the chaotic attractors. Numerical results for the chaotic attractor [Fig. 6(b)] and the limit cycle of $P(f_3)$ (for comparison) are shown in Fig. 7 on logarithmic scales for the embedding dimension ($m=1,2,\ldots,35$). As m increases, the slope ν converges on a constant value. The saturated slopes were determined by the least-squares method within a suitable range of ϵ. We obtained good convergence for large embedding dimensions, and obtained $\nu=3.5$ and 4.2 for the chaotic attractors in Figs. 6(a) and 6(b), respectively.

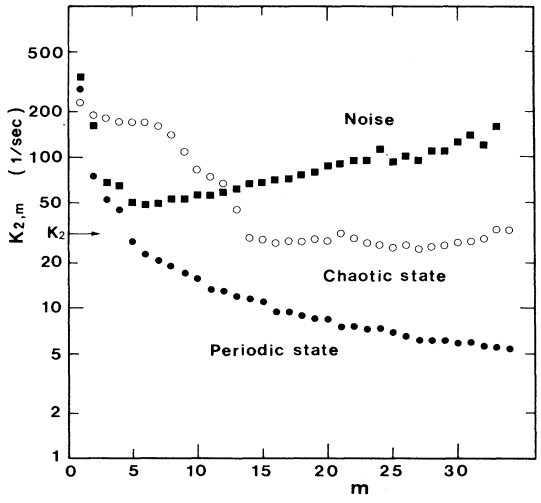

FIG. 8. The entropy parameter $K_{2,m}$ estimated from the correlation integrals as a function of the embedding dimension m for periodic state (●), chaotic state (○), and noise (■). The quantity $K_{2,m}$ converges to a finite and positive value $K_2=0.033$ msec^{-1} for chaotic state and to zero for periodic state, and increases infinitely for noise.

The Kolmogorov entropy, which is the most important measure characterizing chaotic motion, is equal to the sum of positive Lyapunov exponents and can be estimated from the correlation integrals as follows:

$$K_{2,m}=\lim_{\epsilon\to 0}\frac{1}{\tau_d}\log_2\frac{C_m(\epsilon)}{C_{m+1}(\epsilon)}$$

which represents a lower bound of the Kolmogorov entropy for large embedding dimensions. Figure 8 shows the entropy parameter $K_{2,m}$ for the chaotic and periodic motions presented in Fig. 7 as a function of the embedding dimension at a constant ϵ ($\log_2\epsilon=9.17$). The value of $K_{2,m}$ for chaotic motion converges on a finite and stationary value of K_2 over a restricted range of ϵ as the embedding dimension increases. We obtained $K_2\simeq 0.023$ msec^{-1} and $K_2\simeq 0.033$ msec^{-1} for the chaotic attractors corresponding to Figs. 6(a) and 6(b), respectively. When the value of the Kolmogorov entropy is finite and positive, at least one of the Lyapunov exponents must have a positive value and deterministic chaos exists. The value of K_2 for periodic motion tends toward zero, and the value of K_2 at a small range of ϵ [$\log_2\epsilon=6.15$ in Fig. 7(b)], where the slope is not saturated due to statistical noise, shows a tendency to increase infinitely rather than to converge.

B. Forced thermoacoustic states

1. Small-amplitude region: Observation of quenching phenomenon

Keeping the temperature ratio constant ($T_H/T_C\simeq 70.4$), we increased R by gradually increasing the density of the helium gas with no external force applied. After R goes beyond the critical value R ($\simeq 14.4$) a gas column spontaneously oscillates with a small amplitude of the fundamental mode (f_1). The amplitude of the oscillation, which grows rapidly and evenly as R increases, can be controlled by R. For $R\simeq 15.8$ where the

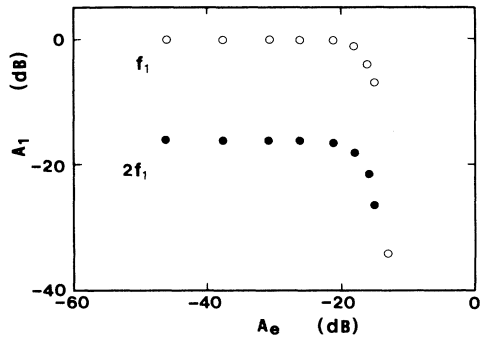

FIG. 9. Signal amplitude A_1 of f_1(○) and $2f_1$(●) vs external driving amplitude A_e. Both of them are normalized by unperturbed signal amplitude of f_1.

instability amplitude is small ($\sim 4.5\times 10^2$ Pa), the external force generates quasiperiodic states with a small number of combination peaks and thin layers of frequency lockings. The forced oscillation, however, can never generate chaotic motion in a gas column when the amplitude is so small. Figure 9 shows the signal amplitude of f_1 and $2f_1$ versus the external driving amplitude, where both amplitudes are normalized by the unperturbed f_1 amplitude. As the external amplitude increases, Taconis oscillation is suddenly quenched and a drastic decrease in its amplitude follows. In a quenching state, all spectral peaks except the forcing peak decrease and eventually become negligible, and the external force starts to dominate the flow in the system completely. Thus, when the Taconis oscillation system is in a small-amplitude region, the chaotic motion is not induced even when the force is strong.

In a moderate-amplitude region, the quenching phenomenon also occurs before the onset of chaos takes place, but the external force does not completely dominate the flow. The system exhibits complex dynamics. To obtain information about the quenching process, we examined the time series strobed with an external force. If the excitation completely dominates the flow, the strobed voltage will be zero. The observed sequence after a sudden decrease in the strobed signal is shown in Fig. 10 for the increases of the external amplitude. Figure 10(a) shows the signal just after the sudden decrease. As A_e increases, the large strobed voltage begins to show many irregular bursts with various heights as shown in Fig. 10(b). The strobed voltage never vanishes even for extremely strong forcing [Fig. 10(c)]. Taconis oscillations with moderate amplitudes are not completely quenched by the external force.

Our observations bear out that there is a minimum amplitude of the instability below which the external force will not induce the quasiperiodic transition to chaos. A multicritical point exists in a generalized parameter space with the amplitudes and frequencies of two oscillators. This space may be divided into small- (including moderate-) and large-amplitude regions. In small- and moderate-amplitude regions, we did not observe the stable critical point which marks the onset of chaos, but did observe the quenching phenomenon caused by an external force. The stable point exists only in the large-amplitude region. This fact bears a striking resemblance to the phenomenon observed in the forced Rayleigh-Bénard convection reported by Stavans [17]. In self-excited systems to which a periodic force is applied, there should exist a critical amplitude of the oscillatory instability between small- and large-amplitude regions, which is dependent on the winding number. Experiments show that the critical amplitude is about 2×10^3 Pa for the golden mean in the Taconis oscillation system.

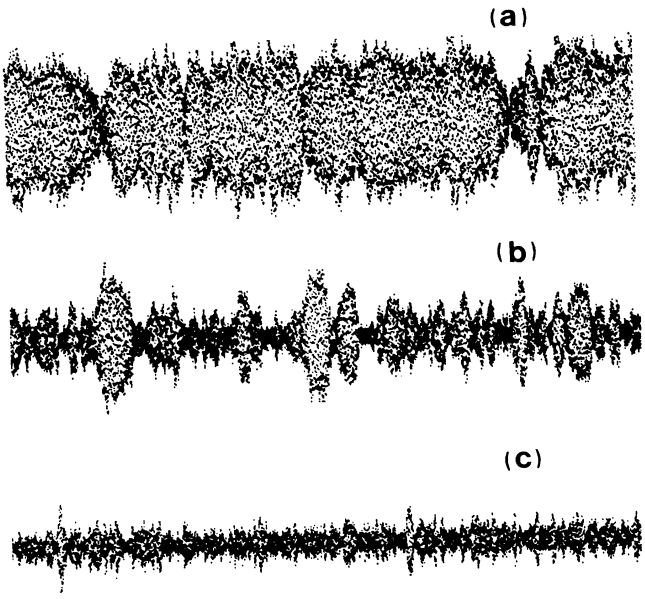

FIG. 10. Observed sequence of strobed pressure voltages when increasing the external force in the moderate amplitude region: (a) the signal just after the onset of a sudden decrease of Taconis oscillation, (b) the irregular burst signal with various heights, and (c) the signal for the extremely strong forcing.

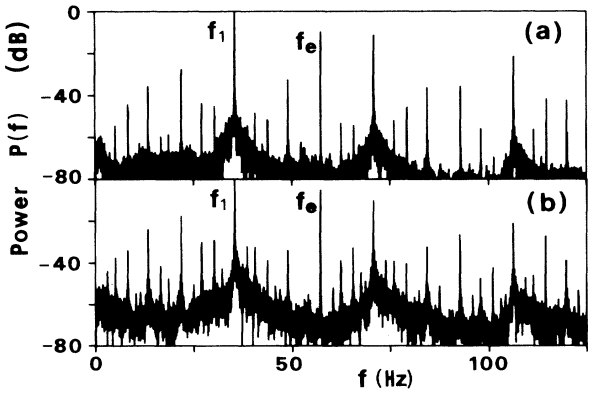

FIG. 11. Power spectra of pressure oscillations for increasing the external force in the large-amplitude region ($R=17.2$): (a) quasiperiodic state below the critical point, and (b) the onset of chaos just at the critical point.

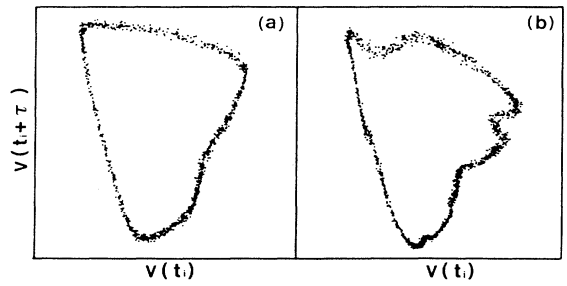

FIG. 12. Experimental Poincaré cross sections projected onto a plane, $V(t_i)$ vs $V(t_i+\tau)$, $(\tau=1/f_e)$: (a) subcritical and (b) critical corresponding to Figs. 11(a) and 11(b), respectively.

2. *Large-amplitude region: Transition from quasiperiodicity to chaos*

For a higher control parameter ($R \simeq 17.2$), the oscillation has an amplitude large enough to produce the onset of chaos. The instability with no external force has an amplitude of 3.2×10^3 Pa. Adjusting the perturbed winding number to the golden mean and keeping the control parameter fixed, we gradually increased the external amplitude. In Fig. 11, we show power spectra below and at the critical point (the point nearest to the onset of chaos). As the amplitude of the external force approaches the critical point, the spectrum shows an increase of about 20 dB of visible noise floor in addition to the increase of higher-order mixing components which consist of the linear combination of f_1 and f_e. Near the critical point, the spectrum contains a great deal of spectral peaks in the low-frequency region. After the onset of chaos is achieved, further increases in the external amplitude do not lead to a further increase of the number of combination peaks, but lead instead to a sudden decrease in spite of the fact that the amplitude is above the critical point. The excitation has a tendency to depress the chaotic motion, and starts to dominate the flow. The system with large amplitudes also exhibits the quenching phenomenon observed in the moderate-amplitude region. The bandwidth of the external amplitude is also dependent on R for the development of chaos.

The experimental determination of the critical point was also confirmed by direct observation of the change in the Poincaré cross section and the self-similar structure of the power spectrum as the most reliable method. Figures 12(a) and 12(b) show subcritical and critical Poincaré cross sections corresponding to Figs. 11(a) and 11(b), respectively, which were reconstructed from the strobed time series $V(t_i)$ $(i=1,2,\ldots,16384)$. The cross sections are nonintersecting in embedding three dimensions, $V(t_i)$, $V(t_i+\tau)$, and $V(t_i+2\tau)$ with $\tau=1/f_e$, and show a well-defined closed loop with no fold for the subcritical, and just above the critical point wrinkles start appearing on the secton and the invariant two-torus is broken down. The apparent folding and break of a torus as evidence of the onset of chaos was observed for larger amplitudes of instability. Figure 13 shows the sequence of Poincaré cross sections below, at, and beyond the critical point observed for $R \simeq 20.4$, where the oscillatory amplitude is 4.6×10^3 Pa.

3. *Universal scaling properties*

The local universal property can be seen in the envelope of the spectral peaks at the low-frequency region. Experimental spectral peaks shown in Figs. 11(a) and 11(b) fall off algebraically as the frequency decreases. We searched the scaling power of f yielding a flat envelope in the low-frequency peaks, and found that the scaling power exists not only at the critical point but also at the subcritical. The data shown in Fig. 11 were reconstructed, and the results are shown in Fig. 14 where the subcritical and critical spectra are divided by f^4 and f^2, respectively, and the scale of the frequency axis is logarithmic. At least the envelope of the spectral peaks for the first generation (labeled 1), which are expressed by all linear combinations of f_1 and f_e with successive coefficients of the Fibonacci sequence (1,1,2,3,5, . . .) for the seed (1,1), is found to be approximately flat in height. The peaks for the critical, belonging to the first generation, can be recognized up to σ^7 in spite of no averaging. Other peaks (labeled by 2,3,4,5) are generated from the Fibonacci sequences with different seeds; for example, peaks labeled 2, 3, 4, and 5 are caused by the sequences with the seeds (2,2), (1,3), (3,3), and (1,4), respectively. Experimental results clearly demonstrate that the scaled power spectrum exhibits a self-similar band structure not only at but also below the critical point, and that as the system approaches the onset of chaos, the scaling power law changes from f^4 to f^2. In the next section (Sec. IV) and the Appendix we will show that such a change of the scaling power law should be attributed to the change of the Poincaré cross section.

Several experiments have been carried out in hydrodynamics (open and closed flow systems) [16,17,27] and solid-state physics [18] in order to find the scaling power of the frequency at the critical point. Previous experi-

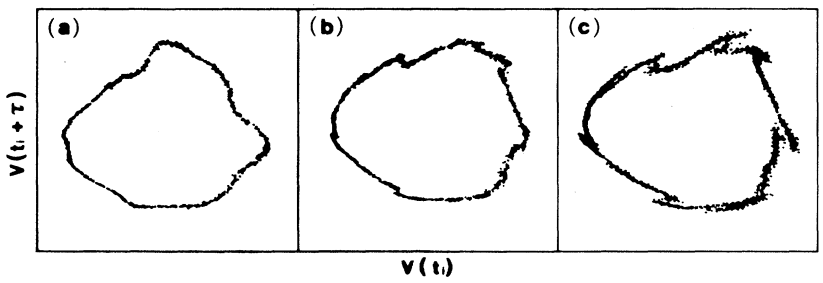

FIG. 13. Experimental Poincaré cross sections projected onto a plane, $V(t_i)$ vs $V(t_i+\tau)$, observed for $R=20.4$: (a) subcritical, (b) critical, and (c) supercritical.

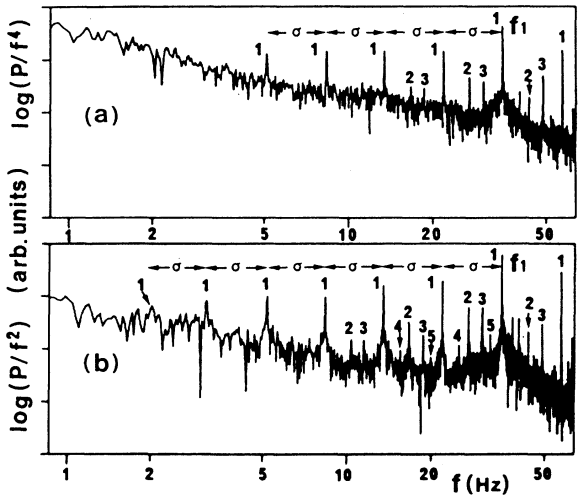

FIG. 14. Experimental scaled power spectra at the golden mean winding number σ: (a) subcritical and (b) critical corresponding to Figs. 11(a) and 11(b), respectively. Spectral peaks labeled by 1, 2, 3, 4, and 5 are generated from the Fibonacci sequences with the seeds (1,1), (2,2), (1,3), (3,3), and (1,4), respectively.

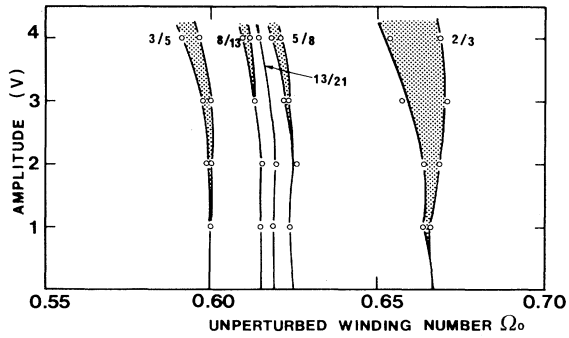

FIG. 15. Experimental frequency-locking diagram (Arnol'd tongues) of driving amplitude A_e vs unperturbed winding number Ω_0.

ments have supported the f^2-scaling power law for the critical except for the experiment by Gwinn and Westervelt [28], who supported the f^4-scaling power law, but have not reported on the scaling for the subcritical. We also tested the universal form seen in the critical power spectrum for a different irrational winding number, the silver mean $\sqrt{2}-1$, and obtained the self-similar spectrum scaled with f^2.

We consider the global scaling universality [20] for the whole set of winding numbers on the critical line. The driving frequency of a synthesizer was slowly swept around the golden mean at a constant external amplitude. Monitoring the Poincaré cross section, we drew up the frequency-locking diagram called "Arnol'd tongues" by varying the external amplitude. The experimental result is shown in Fig. 15 where the boundaries of locked regions ordered in the ratio of the adjacent number of the Fibonacci sequence with the seed (1,1) are mapped out in the space of the external voltage versus the unperturbed winding number $\Omega_0=f_1^0/f_e$ (f_1^0 is the frequency of the instability at no external forcing). Within each tongue, the oscillation f_1 is locked into the driving frequency f_e at $f_1/f_e=p/q$. As the denominator q decreases and the external voltage (nonlinearity K) increases, the tongues increase in width. This property is equivalent to that of the phase diagram predicted by the sine circle map. We focus our attention on the locking structure, the widths of tongues on the critical line ($K=1$) where a complete devil's staircase is formed. It is theoretically predicted that the tongues form a Cantor-type set with a fractal dimension of $D=0.868$ on the critical line. The dimension D characterizing the scaling of the locking structure was *estimated* from the equation $\sum_i (S_i/S)^D \simeq 1$ where S is the distance between two locked-band parents around an irrational winding number and S_i are the distance between adjacent tongues (including in the parent) constructed according to a Farey composition. The experimental critical line, however, is not flat for a whole winding number. It depends on Ω_0. Therefore, we locally estimated the dimension around the golden mean at a constant external amplitude. The $\frac{3}{5}$ and $\frac{5}{8}$ tongues were selected as two parents and only one $\frac{8}{13}$ tongue as the daughter. The observed intervals of S, S_1, and S_2 were 55.79–57.77, 55.79–56.60 and 56.76–57.77 Hz, respectively. Thus, we obtained $D=0.89$ with an experimental error of ± 0.02. The experimental value close to theoretical $D=0.868$ was obtained for a higher amplitude of instability where, as the driving amplitude increases, the dimension decreases as follows: for the driving amplitudes of 2.0, 2.4, and 3.0 V, D takes 0.92, 0.90, and 0.87, respectively. The same universal number D was also obtained in other hydrodynamical experiments, Rayleigh-Bénard convections in mercury [17], ^{3}He–superfluid–^{4}He mixture [29], and open flow system [27].

The fractal structure is seen in the critical Poincaré cross section itself. The critical attractors shown in Figs. 12(b) and 13(b) are constructed not from a part with homogeneous density of points but from some parts with high and low concentration of points. A global scaling property of the attractors with density variation is characterized by the multifractal spectrum $f(\alpha)$ [21], which is a fractal dimension of the set of the singularity with scaling index α. To calculate $f(\alpha)$ efficiently from short data sets including a small drift during the experiment, we used an indirect method, recurrence-time approximation, proposed by Jensen and co-workers [21]. The probability $P_i(l)$ that other points fall within a small distance l of a given point i on the Poincaré cross section was estimated by the inverse of the averaged recurrence time $m_i(l)$ for a few points. According to whether the concentration of points is high or low, the recurrence time is short or long, respectively. We determined the $f(\alpha)$ for the critical Poincaré cross section using the relation for a small distance l,

$$\Gamma(q,l)=\langle m_i(l)^{1-q}\rangle \sim l^{\tau(q)} ,$$

where the angular brackets show the average overall points ($\sim$3000 points). Figure 16 shows the log-log plots

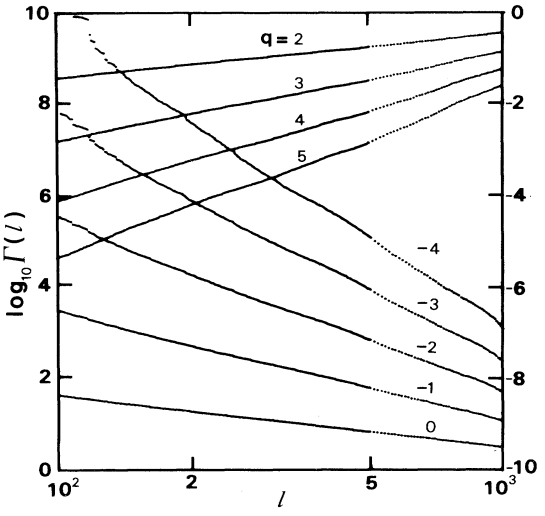

FIG. 16. Log-log plots of $\Gamma(q,l)$ vs l for several values of q. $\Gamma(q,l)$ for negative and positive q obeys the left- and right-hand scales, respectively.

of $\Gamma(q,l)$ versus l for several values of q, where the range of l represented corresponds to 2–25% of the largest separation between two points on the attractor. For many values of q, we found the scaling exponent $\tau(q)$ by fitting the log-log plots to a straight line using the least-squares method in a reasonable scaling region of l (for example, we selected $150 \leq l \leq 450$ for $q=-2$), below which noise effects become dominant. The $f(\alpha)$ spectrum was calculated from $\tau(q)$ through the Legendre transformation,

$$\alpha = \frac{d\tau(q)}{dq} ,$$

$$f(\alpha(q)) = q\alpha - \tau(q) .$$

The experimental results for $f(\alpha)$ versus α are shown in Fig. 17, where solid circles, open circles, and triangle marks represent the critical, subcritical, and supercritical Poincaré cross sections corresponding to Figs. 12(b), 12(a), and 13(c), respectively. The solid curve is the theoretical $f(\alpha)$ spectrum defined by the sine circle map at the critical point and at the golden mean winding number. The agreement of the critical $f(\alpha)$ between the experiment and the theory means that Taconis oscillation belongs to the same universality class as the sine circle map in spite of the complexity of thermoacoustics.

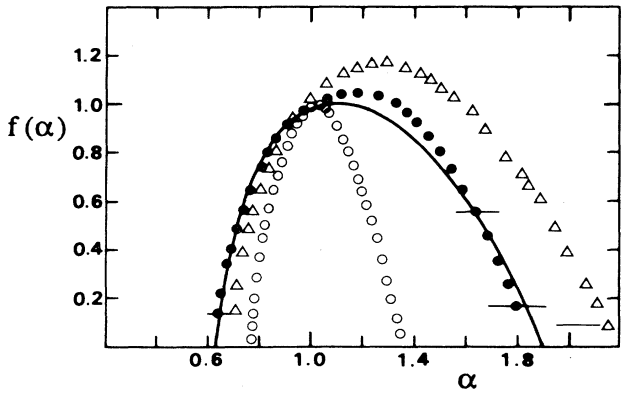

FIG. 17. Experimental $f(\alpha)$ spectra for subcritical (○), critical (●), and supercritical (Δ). The solid curve is theoretical $f(\alpha)$ predicted by the sine circle map at the golden mean winding number and at the onset of chaos.

The subcritical $f(\alpha)$ spectrum tends to narrow and its maximum point shifts slightly toward $\alpha=1$. The tendency for the spectrum to narrow and shift has also been observed in Rayleigh-Bénard convection [21,29] and an electronic resonator system [15]. Subcritical attractors do not have the multifractal structure, and in principle the subcritical $f(\alpha)$ should be trivial. It collapses to a point at $f(1)=1$. Experimentally, a small deviation from the criticality causes the width of $f(\alpha)$ to narrow considerably. Using the sine circle map, Arneodo and Holschneider [30] showed that the nontrivial spectrum for the subcritical is due to a finite number of data points. The supercritical spectrum exhibits an increase of the top value of $f(\alpha)$ (indicating an increase of the Hausdorff dimension) and a shift to the right of the maximum scaling index α.

The sine circle map can effectively describe the behavior of a forced thermoacoustics system at least up to the onset of chaos. However, the universal scaling properties for supercritical attractors strongly folded can no longer be described by the one-dimensional circle map. Now we are interested in the universality beyond the onset of chaos predicted by Gunaratne and coworkers [31] who suggest that low-dimensional strange attractors can be categorized into several classes characterized by universal topological features.

IV. DISCUSSION

Shenker and Ostlund and co-workers [19] have theoretically predicted that the critical power spectrum for a time series given by iterating the sine circle map ($K=1$) shows a self-similar hierarchical structure on the log-log plots of the power scaled with f^2 versus the frequency. To test the applicability of such a fascinating prediction, Fein, Heutmaker, and Gollub [16] performed the experiment in the thermally modulated Rayleigh-Bénard convection system, and confirmed the f^2-scaling power law. Subsequent experiments [17,18,27] have also supported this scaling power law for the angle, except for the work in solid-state physics [28]. Fein, Heutmaker, and Gollub and Mori [32], however, suggested that the observable should correspond to the projection along an axis in the phase space rather than the angle itself. The envelope of the spectral peaks for the projection follows the scaling with a different power law; that is, at the critical point, the envelope is found to be scaled with a higher-order power f^4 [16]. The f^4 scaling is clearly different from the experimental fact. Which variable of the map is equivalent to the observable, the angle or its projection? Experimental results regarding the change of the scaling power law from f^4 to f^2 may offer the key to answer this question. In the Appendix we give a numerical explanation of the results, and show that the change from f^4 to

f^2 is attributed to the change of the Poincaré cross section from a mild to a sharp wrinkle. Important features are that the scaling law obtained is derived from the projection and exists not only at the critical point but also at the subcritical one. It is our belief that the f^2 scaling observed in other systems is also attributable to the same origin. As an answer to the question stated above we assert that the empirical variable does behave like the projection in the phase space.

V. CONCLUSIONS

We have presented experimental data on thermoacoustics oscillations in which spontaneous states and externally forced states are observed to exhibit quasiperiodic and chaotic dynamics. In spontaneous states, chaotic motions arise from competition between three different oscillatory modes simultaneously induced with incommensurate frequencies. As a route to chaos, stable three-frequency quasiperiodicity was found to exist before the onset of chaos. We analyzed experimental time series using techniques of nonlinear dynamical theories, and determined the correlation dimension ν and the entropy K_2 of chaotic attractors. Typical values were $\nu=4.2$ and $K_2=0.033$ msec^{-1} for the three-frequency route, and $\nu=3.5$ and $K_2=0.023$ msec^{-1} for the two-frequency route.

A spontaneous state was periodically perturbed by the external force. In forced states, we found that the instability with a small amplitude is quenched by strong forcing, and stable critical points for the onset of chaos exist only in the large-amplitude region. We tested whether the local and global universal properties predicted by the sine circle map for the quasiperiodic transition to chaos are applicable to thermoacoustic systems. We have presented some experimental evidence in favor of the relevance of the map universality: (1) the self-similar and scaling power spectrum at the golden mean, (2) the fractal dimension $D=0.89\pm0.02$ of the locking structure on the critical line, and (3) the multifractal spectrum for the golden torus. In particular, we found that the scaling power law yielding a flat envelope of spectral peaks changes from f^4 to f^2 as the system approaches the onset of chaos. It was numerically confirmed that the change of the scaling power is due to the change of the Poincaré cross section from a mild to a sharp wrinkle.

Recently the concept of thermoacoustics has been of great interest in many physical systems, astronomy, fields of application to a new type of refrigerator, and so on. The applicability of the map universality to the system will enable us to effectively predict the qualitative and quantitative behavior of nonlinear thermoacoustic phenomena even if basic equations are not known or if they are too difficult to solve. I believe that the experimental results presented in this paper are important for the development and application of thermoacoustics in the future.

ACKNOWLEDGMENTS

This work was performed at the Instrument and the Cryogenic Centers, the Institute of Molecular Science, and supported by Grants-in-Aid for Scientific Research from the Ministry of Education, Science and Culture (Nos. 03640347 and 04452056) and a grant from the Ishida Foundation (Grant No. 91-538). Very stimulating discussions with Professor H. Mori, Professor T. Yamada, Professor H. Mamada, and Professor K. Fukushima are gratefully acknowledged. I would like to thank K. Hayasaka, K. Kato, and T. Takayama for the preparation of liquid helium during this experiment, and the members of the Narahara laboratory at the University of Tsukuba for their advice and encouragement.

APPENDIX

All behavior from a torus to chaos cannot be completely described by the circle map alone. We need to capture the property of wrinkles appearing on a torus near the onset of chaos. Typical examples were presented in Figs. 12 and 13, where wrinkles develop from mild to sharp as the system approaches the onset. We used the simple model proposed by Antoranz and Mori [33] to consider the radial motion characterizing wrinkles on a torus. The radius $R(\theta_n)$ of the Poincaré cross section is provided by $R_1(\theta_n)=1+a\sin(m\pi\theta_n)$ or $R_2(\theta_n)=1+a\cos(m\pi\theta_n)$, where a is a parameter with a nonzero value and m is an odd number. The model $R_1(\theta_n)$ presents a continuous closed curve with a mild wrinkle characterizing the subcritical Poincaré cross section. The model $R_2(\theta_n)$ gives a critical cross section characterized by a sharp wrinkle, and produces a discontinuous change $R_2(0)-R_2(1)=2a$. For the angle $\theta_n(\mathrm{mod}1)$ we used the sine circle map. The dressed winding number was always adjusted to the golden mean. We calculated power spectra of the Cartesian coordinates, $X_1=R_1(\theta_n)\cos(2\pi\theta_n)$ and $X_2=R_2(\theta_n)\cos(2\pi\theta_n)$. Power spectra of X_1 and X_2

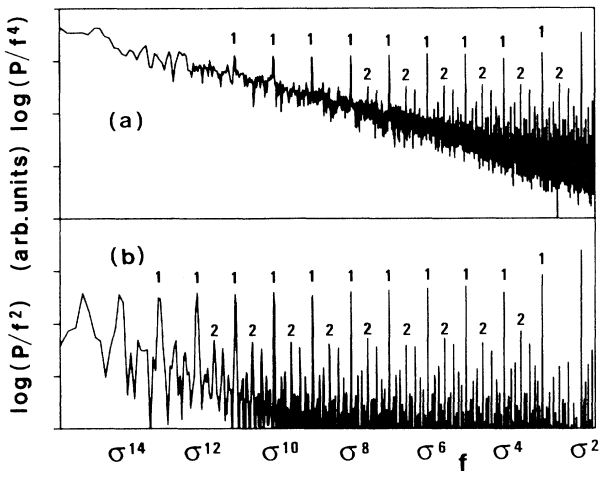

FIG. 18. Scaled power spectra of $X=R\cos(2\pi\theta_n)$ at the golden mean winding number: (a) $R=(R_1)=1+0.5\sin(\pi\theta_n)$ and (b) $R(=R_2)=1+0.5\cos(\pi\theta_n)$. The angle θ_n follows the sine circle map with $K=0.5$ and $\Omega_0=0.614\,526\,4\ldots$ for (a) and $K=1$ and $\Omega_0=0.606\,661\,0\ldots$ for (b). The scaling power law follows f^4 or f^2 according as the radius R is R_1 or R_2.

compare well with those of time series below and at the critical point, respectively. Figure 18(a) shows the scaled power spectrum for X_1 on a log-log plot, where we select $a=0.5$, $m=1$, $K=0.5$, and $\Omega_0=0.614\,526\,4\ldots$. The height of the spectral peaks is found to be proportional to f^4. Figure 18(b) shows this for X_2 with a sharp wrinkle, where we select $a=0.5$, $m=1$, $K=1$, and $\Omega_0=0.606\,661\,0\ldots$. The scaling power law of the frequency yielding a flat envelope is f^2, which is the same as the power law of the angle predicted by Ostlund *et al.* [19]. We tested the power law for other kinds of functions $R(\theta_n)$, other values of a, and a different irrational winding number, the silver mean. It was confirmed that the scaled power spectrum has a self-similar structure in all cases and that its envelope follows the power law f^2 if the Poincaré cross section has a sharp wrinkle with a discontinuity. Antoranz and Mori [33] numerically found the same power law for the linear map ($K=0$).

*FAX: 0566-36-4337.

[1] C. Sondhauss, Ann. Phys. (Leipzig) **79**, 1 (1850); J. W. Strutt and Lord Rayleight, *Theory of Sound* (Dover, New York, 1945), Sec. 322i; K. T. Feldman, Jr., J. Sound Vib. **7**, 71 (1968).

[2] P. L. Rijke, Ann. Phys. (Leipzig) **107**, 339 (1859); K. T. Feldman, Jr., J. Sound Vib. **7**, 83 (1968).

[3] J. C. Wheatly and A. Cox, Phys. Today **38** (8), 50 (1985); J. C. Wheatly, T. Hofler, G. W. Swift, and A. Migliori, Phys. Rev. Lett. **50**, 499 (1983); J. Acoust. Soc. Am. **74**, 153 (1983); Am. J. Phys. **53**, 147 (1985).

[4] W. H. Keesom, *Helium* (Elsevier, Amsterdam, 1942), p. 174; C. F. Squire, *Low Temperature Physics* (McGraw-Hill, New York, 1953), p. 23; K. W. Taconis, J. J. M. Beenakker, A. O. C. Nier, and L. T. Aldrich, Physica **15**, 733 (1949) (see footnote on p. 738).

[5] N. Rott, Z. Angew. Math. Phys. **20**, 230 (1969); **24**, 54 (1973); Adv. Appl. Mech. **20**, 135 (1980).

[6] T. Yazaki, A. Tominaga, and Y. Narahara, J. Low Temp. Phys. **41**, 45 (1980).

[7] G. W. Swift, J. Acoust. Soc. Am. **84**, 1145 (1988).

[8] A. Tominaga, Y. Narahara, and T. Yazaki, J. Low Temp. Phys. **54**, 233 (1984); A. Tominaga, in *Proceedings of the Third Japanese-Sino Joint Seminar on Small Refrigerator and Related Topics, Okayama, Japan, 1989* (Cryogenic Society of Japan and Academia Sinica, Tokyo, 1989), p. 141.

[9] T. Yazaki, S. Sugioka, F. Mizutani, and H. Mamada, Phys. Rev. Lett. **64**, 2515 (1990); T. Yazaki, S. Takashima, and F. Mizutani, *ibid.* **58**, 1108 (1987).

[10] C. Grebogi, E. Ott, and J. A. York, Phys. Rev. Lett. **51**, 339 (1983); Physica **15D**, 334 (1985).

[11] J. P. Gollub and S. V. Benson, J. Fluid Mech. **100**, 449 (1980); A. Libchaber, S. Fauve, and C. Laroche, Physica **7D**, 73 (1983); S. Martin, H. Leber, and W. Martienssen, Phys. Rev. Lett. **53**, 303 (1984);. A. Cumming and P. S. Linsay, *ibid.* **60**, 2719 (1988).

[12] H. L. Swinney, Physica **7D**, 3 (1983); P. Bergé, Y. Pomeau, and C. Vidal, *Order Within Chaos: Towards a Deterministic Approach to Turbulence* (Hermann, Paris, 1984); H. G. Schuster, *Deterministic Chaos* (VCH, Weinheim, 1988).

[13] J. Glazier and A. Libchaber, IEEE Trans. Circuits Syst. **35**, 790 (1988).

[14] D. D'Humieres, M. R. Beasley, B. A. Huberman, and A. Libchaber, Phys. Rev. A **26**, 3483 (1982); F. C. Moon, J. Cusumano, and P. J. Holmes, Physica **24D**, 383 (1987).

[15] Z. Su, R. W. Rollins, and E. R. Hunt, Phys. Rev. A **36**, 3515 (1987); **40**, 2689 (1989); **40**, 2698 (1989).

[16] A. P. Fein, M. S. Heutmaker, and J. P. Gollub, Phys. Scr. **T9**, 79 (1985).

[17] J. Stavans, F. Heslot, and A. Libchaber, Phys. Rev. Lett. **55**, 596 (1985); J. Stavans, Phys. Rev. A **35**, 4314 (1987).

[18] E. G. Gwinn and R. M. Westervelt, Phys. Rev. Lett. **57**, 1060 (1986); **59**, 157 (1987); G. A. Held and C. Jeffries, *ibid.* **56**, 1183 (1986).

[19] S. J. Shenker, Physica **5D**, 405 (1982); M. J. Feigenbaum, L. P. Kadanoff, and S. J. Shenker, *ibid.* **5D**, 370 (1982); D. Rand, S. Ostlund, J. Sethna, and E. Siggia, Phys. Rev. Lett. **49**, 132 (1982); S. Ostlund, D. Rand, J. Sethna, and E. Siggia, Physica **8D**, 303 (1983).

[20] M. H. Jensen, P. Bak, and T. Bohr, Phys. Rev. Lett. **50**, 1637 (1983); Phys. Rev. A **30**, 1960 (1984); P. G. E. Hentschel and I. Procaccia, Physica **8D**, 435 (1983); P. Cvitanovic, M. H. Jensen, L. P. Kadanoff, and I. Procaccia, Phys. Rev. Lett. **55**, 343 (1985).

[21] M. H. Jensen, L. P. Kadanoff, A. Libchaber, I. Procaccia, and J. Stavans, Phys. Rev. Lett. **55**, 2798 (1985); J. A. Glazier, G. Gunaratne, and A. Libchaber, Phys. Rev. A **37**, 523 (1988); T. C. Halsey, M. H. Jensen, L. P. Kadanoff, I. Procaccia, and B. I. Shraiman, *ibid.* **33**, 1141 (1986); T. C. Halsey and M. H. Jensen, Physica **23D**, 112 (1986).

[22] H. Yamazaki and M. Mino (private communication); Prog. Theor. Suppl. **98**, 400 (1989).

[23] T. Yazaki, A. Tominaga, and Y. Narahara, J. Heat Transfer. **105**, 889 (1983); U. Kurzweg and L. D. Zhao, Phys. Fluids **27**, 2624 (1984).

[24] W. Chester, J. Fluid Mech. **18**, 44 (1964); A. B. Coppens and J. V. Sanders, J. Acoust. Soc. Am. **43**, 516 (1968); D. B. Cruikshank, *ibid.* **52**, 1024 (1972).

[25] N. Packard, J. P. Crutchfield, J. D. Farmer, and R. S. Shaw, Phys. Rev. Lett. **45**, 712 (1980); F. Takens, in *Dynamical Systems and Turbulence,* edited by D. A. Rand and L-S. Young, Lecture Notes in Math Vol. 898 (Springer, Heidelberg, 1981), p. 366.

[26] P. Grassberger and I. Procaccia, Phys. Rev. Lett. **50**, 346 (1983); Phys. Rev. A **28**, 2591 (1983).

[27] D. J. Olinger and K. R. Sreenivasan, Phys. Rev. Lett. **60**, 797 (1988).

[28] E. G. Gwinn and R. M. Westervelt, Phys. Rev. Lett. **59**, 247 (1987).

[29] R. Mainieri, T. S. Sullivan, and R. E. Ecke, Phys. Rev. Lett. **63**, 2357 (1989); R. E. Ecke, R. Mainieri, and T. S. Sullivan, Phys. Rev. A **44**, 8103 (1991).

[30] A. Arneodo and M. Holschneider, Phys. Rev. Lett. **58**, 2007 (1987).

[31] G. H. Gunaratne, P. S. Linsay, and M. J. Vinson, Phys. Rev. Lett. **63**, 1 (1989); G. H. Gunaratne, M. H. Jensen, and I. Procaccia, Nonlinearity **1**, 157 (1988).

[32] H. Mori (private communication).

[33] J. C. Antoranz and H. Mori, Physica **16D**, 184 (1985).